GEOPHYSICS, VOL. 80, NO. 1 (JANUARY-FEBRUARY 2015); P. Q1–Q13, 19 FIGS., 1 TABLE.
10.1190/GEO2014-0181.1

Studying CO_2 storage with ambient-noise seismic interferometry: A combined numerical feasibility study and field-data example for Ketzin, Germany

Boris Boullenger[1], Arie Verdel[2], Bob Paap[2], Jan Thorbecke[1], and Deyan Draganov[1]

ABSTRACT

Seismic interferometry applied to ambient-noise measurements allows the retrieval of the seismic response between pairs of receivers. We studied ambient-noise seismic interferometry (ANSI) to retrieve time-lapse reflection responses from a reservoir during CO_2 geologic sequestration, using the case of the experimental site of Ketzin, Germany. We applied ANSI to numerically modeled data to retrieve base and repeat reflection responses characterizing the impedances occurring at the reservoir both with and without the injection of CO_2. The modeled data represented global transmission responses from band-limited noise sources randomly triggered in space and time. We found that strong constraints on the spatial distribution of the passive sources were not required to retrieve the time-lapse signal as long as sufficient source-location repeatability was observed between the base and the repeat passive survey. To illustrate the potential of the technique, ANSI was applied to three days of passive field data recorded in 2012 at Ketzin. Comparison with the modeled results illustrated the potential to retrieve key reflection events using ANSI on field data from Ketzin. This study supports the idea that the geologic setting and characteristics of ambient noise at Ketzin may be opportune to monitor CO_2 sequestration.

INTRODUCTION

Ambient-noise seismic interferometry (ANSI) can be defined as the process of retrieving the seismic response between a pair of sensors, to obtain a virtual source at the position of one of the sensors, by crosscorrelating the responses from passive seismic sources. For analysis of reflected-wave ANSI, the starting point is the classic paper by Claerbout (1968) in which he shows that the autocorrelation of the global transmission response (direct arrivals, internal, and free-surface multiples; see Wapenaar et al., 2010) of a layered medium gives the plane-wave reflection response of that medium. He conjectures that this result could also be applied to the 3D situation using crosscorrelation. The conjecture was later analyzed using the powerful method of stationary phase (Schuster, 2001; Schuster et al., 2004; Snieder, 2004; Schuster and Zhou, 2006). Claerbout's 1D result has since been generalized to 3D (Wapenaar, 2004). An excellent interdisciplinary review of the correlation properties of random wavefields is provided by Larose et al. (2006).

In ANSI for body-wave reflection retrieval, the passive measurements are lengthy records that have registered many global transmission responses from unknown noise sources. ANSI has been applied by various authors at exploration scale to retrieve reflection images (e.g., Draganov et al., 2007, 2009, 2013; Nakata et al., 2011; Xu et al., 2012). Because no active sources are deployed in ANSI, time-lapse application of this technique could allow cost-effective monitoring of reservoirs such as in the case of CO_2 storage. Other authors apply ANSI to fluid-solid interface waves to monitor offshore CO_2 storage projects (e.g., de Ridder and Biondi, 2012).

Time-lapse seismic data are widely used to monitor hydrocarbon reservoirs by repeating active acquisition surveys. The multiple vintage reflection data sets are processed to reveal reflectivity changes expressed by amplitude variations and time shifts as a function of time. For projects aimed at geologic CO_2 storage, the time-lapse

Manuscript received by the Editor 17 April 2014; revised manuscript received 5 August 2014; published online 30 December 2014.
[1]Delft University of Technology, Department of Geoscience and Engineering, Delft, The Netherlands. E-mail: b.boullenger@tudelft.nl; d.s.draganov@tudelft.nl; j.w.thorbecke@tudelft.nl.
[2]TNO, Utrecht, The Netherlands. E-mail: arie.verdel@tno.nl; bob.paap@tno.nl.

data are used to monitor the CO_2 saturation changes in the target reservoir and prevent potential leakage (e.g., Arts et al., 2004). A potential advantage of ANSI over controlled-source time-lapse surveying is that the source-receiver geometry of the retrieved reflection responses is exactly repeated, provided that the seismic stations are permanently installed. Moreover, time-lapse ANSI would not generate any costs for the repeated deployment of active sources and long-term planning. However, similar to controlled-source time-lapse surveying, significant distortions may occur in the time-lapse signal due to the nonexact repetition of the (passive) seismic source characteristics. Ugalde et al. (2013) also propose to use passive recording above a CO_2 storage site for monitoring. The authors propose to first use ANSI for retrieval of coda waves and then to apply coda-wave interferometry to possibly detect small velocity changes in the subsurface.

In this study, we aim at assessing numerically the feasibility of time-lapse monitoring of the CO_2 reservoir at Ketzin using ANSI. First, we present the characteristics of the CO_2 storage site at Ketzin and of the receiver array installed in the field. Then, we recall the ANSI relations. Next, we describe our modeling approach for simulating long passive measurements and apply crosscorrelations to the numerically modeled passive data to obtain time-lapse virtual shot gathers corresponding to two CO_2 saturation scenarios. We investigate the conditions for the recorded body-wave noise needed to obtain an accurate time-lapse difference and discuss several recommendations to apply time-lapse ANSI successfully to field data. Finally, we apply ANSI by autocorrelation to passive field data after CO_2 has been injected. We compare the results obtained from the numerically modeled passive data with the results from this field survey — we compare an autocorrelation panel of modeled noise with autocorrelated panels of noise as recorded with buried sensors from the permanent array installed in the field at Ketzin.

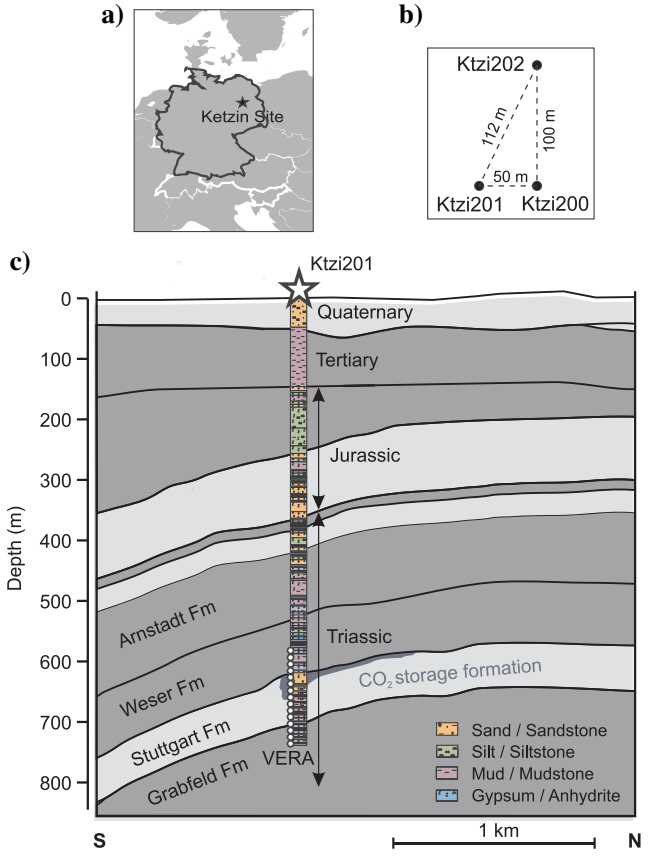

Figure 1. (a) Geographical location of Ketzin. (b) Map view of the surface locations of injection well Ktzi201 and monitoring wells Ktzi200 and Ktzi202. (c) Schematic north–south section through the Ketzin anticline. Modified from Bergmann et al. (2014).

CO_2 STORAGE SITE AND FIELD DATA

From the start of the CO_2 injection in 2008 to the end of the injection in August 2013, more than 67,000 tons of CO_2 were injected at the demonstration site for geologic storage near the town of Ketzin in Germany. Ketzin is located in the northeast German Basin, a subbasin of the Central European basin system. The abundance of well data in the area provides a relatively good understanding of the geologic structure and lithostratigraphy (Förster et al., 2006). Injection well Ktzi201 is located on the southern flank of a gently dipping anticline (Figure 1). The target reservoir for CO_2 is the Upper Triassic Stuttgart Formation in a saline aquifer, located at a depth of around 650 m. The Stuttgart Formation is, on average, 80 m thick and lithologically heterogeneous: Sandstones of good reservoir quality alternate with mudstones of poor reservoir quality (Förster et al., 2009). Claystones, silty claystones, and anhydrite form an approximately 200-m-thick section above the Stuttgart Formation. The 10–20-m-thick anhydrite layer representing the upper part of this section (Förster et al., 2006) is mapped as a clear reflection on seismic surveys and commonly labeled as K2 reflector (see Figure 2). This is actually the composite response from the anhydrite top and bottom boundaries. The high-impedance anhydrite formation lies about 80 m above the top of the Stuttgart Formation.

To monitor the migration of the CO_2 plume during the injection process, several geophysical measurements were conducted in boreholes as well as at the surface, including time-lapse reflection seismics (with surface acquisition). The work of Ivandic et al. (2013) on time-lapse active seismic surveys shows significant evidence of durable impedance changes at the target reservoir.

As part of the monitoring experiments, The Netherlands Organization for Applied Scientific Research (TNO) installed a permanent array of seismic sensors near the injection well in 2009 (Figure 3). As depicted in Figure 4, this array is composed of 3C geophones and hydrophones divided in three lines: a horizontal line at the surface, another one at a depth of 50 m, and a vertical line that connects the previous two. The geometry of the array favors high-resolution recording and provides a high signal-to-noise ratio for the data recorded at the buried sensors. The limited extension of the array is, however, not optimal for microseismic source localization. This was realized at the start of the project, but better alternatives were not available due to practical considerations. Since its installation, the array has recorded passive seismic data continuously. First analysis of these long ambient-noise records showed that, although surface-wave energy is dominant in many parts of the passive records, some time periods of the records have dominant body-wave noise and sometimes contain clear body-wave energy traveling upward (Santonico et al., 2012). These observations are encouraging because measurements of body-wave energy are required to retrieve reflections with ANSI (Almagro Vidal et al., 2014). Xu et al. (2012) apply

ANSI at Ketzin on passive data collected during 25 h at a temporary line of surface receivers. By applying crosscorrelation on selected and filtered noise panels containing dominant body waves, they retrieved virtual reflection data that they migrate to obtain an image. Although their total length of noise records was limited to 25 h, their result shows that reflections obtained with ANSI coincide with the ones obtained from an active survey. This is clear evidence of significant body-wave noise at Ketzin that could be used to retrieve time-lapse reflection data.

AMBIENT-NOISE SEISMIC INTERFEROMETRY BY CROSSCORRELATION

Wapenaar and Fokkema (2006) use Green's function (or seismic impulse response) representations to derive seismic interferometry relations for applications with passive data. As represented in Figure 5, we consider shallow-buried receivers at positions $\mathbf{x}_A$ and $\mathbf{x}_B$, and a subsurface source boundary S that, together with the earth's free surface, encloses them. In the acoustic situation, the Green's function between the pair of receivers can be derived in terms of crosscorrelations and integration. The crosscorrelations are performed over recordings of the Green's functions at the receivers from the sources along the integration boundary S. In the frequency domain, this relation is

$$\hat{G}(\mathbf{x}_B, \mathbf{x}_A, \omega) + \hat{G}^*(\mathbf{x}_B, \mathbf{x}_A, \omega) \approx \frac{2}{\rho c} \oint_S \hat{G}^*(\mathbf{x}_B, \mathbf{x}, \omega) \hat{G}(\mathbf{x}_A, \mathbf{x}, \omega) d^2\mathbf{x}, \quad (1)$$

where $\mathbf{x}$ is the boundary-source coordinate; and ρ and c are the constant mass density and propagation velocity, respectively, along S; $\hat{G}(\mathbf{x}_A, \mathbf{x}, \omega)$ and $\hat{G}(\mathbf{x}_B, \mathbf{x}, \omega)$ are, respectively, the Green's functions from a source at $\mathbf{x}$ to a receiver at $\mathbf{x}_A$ and to a receiver at $\mathbf{x}_B$; whereas $\hat{G}(\mathbf{x}_B, \mathbf{x}_A, \omega)$ is the Green's function from $\mathbf{x}_A$ to $\mathbf{x}_B$. The * sign denotes complex conjugation and corresponds to time reversal in the time domain. Equation 1 holds for an inhomogeneous nondissipative medium enclosed by S and demonstrates the potential to retrieve the seismic response at $\mathbf{x}_B$, as if from a virtual source at $\mathbf{x}_A$, using recordings at $\mathbf{x}_A$ and $\mathbf{x}_B$. Implicit assumptions in the above relation (but explicit during the derivation in Wapenaar and Fokkema, 2006) are that S has a very large radius, such that the specular rays always nearly coincide with the normal to S (far-field approximation), that the medium is smooth in the vicinity of S and homogeneous outside S.

For real field case situations, several deviations of the above-mentioned assumptions may occur. If the latter assumption is not met and scattered energy from inhomogeneities outside the domain enclosed by the source distribution is recorded at the receivers, spurious events will also be present in the resulting crosscorrelation

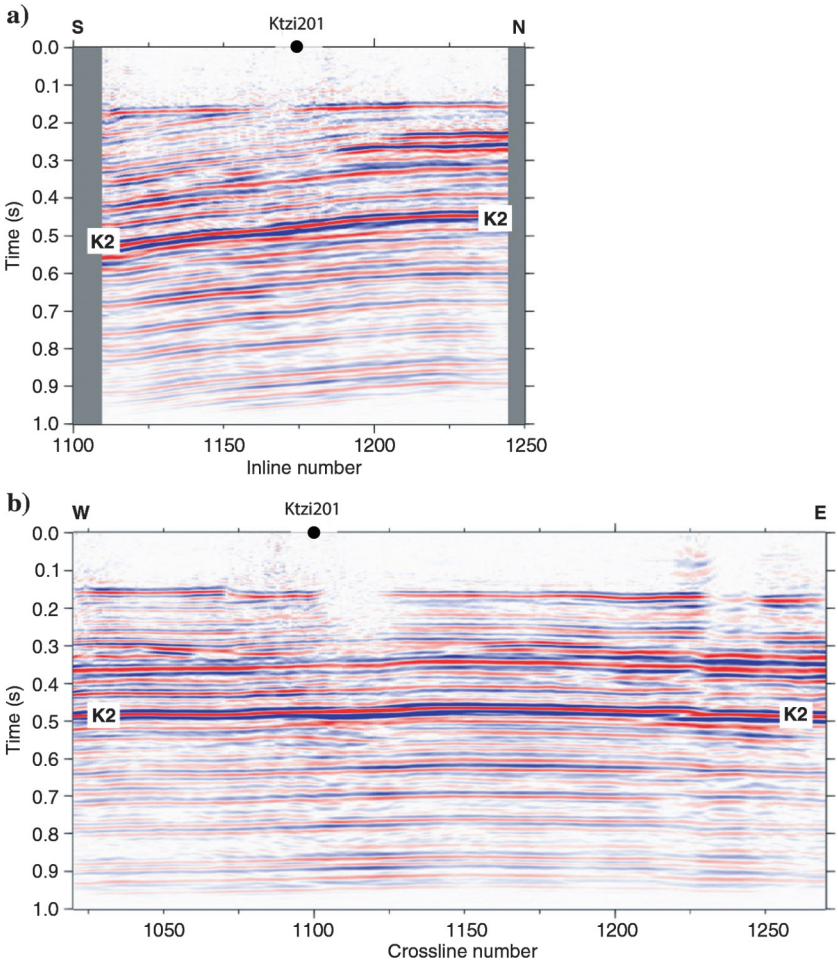

Figure 2. Time-migrated slices from a 3D seismic subvolume (see Juhlin et al., 2007) with K2 indicated as the marker reflector: (a) north–south (crossline 1100) slice and (b) east–west (inline 1175) slice. The north–south and the east–west sections are approximately 4 and 6 km wide, respectively. The black dot marks the location of the injection well (Ktzi201). The orientation of the TNO array is approximately east–west, namely, along the strike direction of the anticline. Modified from Juhlin et al. (2006).

signal together with an estimate of $\hat{G}(\mathbf{x}_B, \mathbf{x}_A, \omega)$ (Wapenaar and Fokkema, 2006). However, the events emerging after crosscorrelation that are caused by the inhomogeneities outside S will interfere destructively if S is sufficiently irregular (as is the case for randomly distributed sources), leading to a suppression of the retrieval of spurious energy and consequently a more correct estimate of $\hat{G}(\mathbf{x}_B, \mathbf{x}_A, \omega)$ (Draganov et al., 2004).

In practice, the assumption of S having a vary large radius is unlikely to be met. Apart from the possible occurrence of spurious events, this would result in amplitude errors for $\hat{G}(\mathbf{x}_B, \mathbf{x}_A, \omega)$ that may be significant, as compared with the true Green's function (Ramirez and Weglein, 2009). Also note that in practical applications of ANSI, the factor $2/\rho c$ is disregarded because it has no effect on the retrieved response in terms of phase and kinematics. To adopt a representation for ambient noise measurements, we disregard the assumption of impulse signals, implicit in equation 1, and consider mutually uncorrelated noise signatures, as given by

$$\langle \hat{N}(\mathbf{x}, \omega) \hat{N}^*(\mathbf{x}', \omega) \rangle = \delta(\mathbf{x} - \mathbf{x}', \omega) \hat{S}(\omega), \qquad (2)$$

where $\hat{N}(\mathbf{x}, \omega)$ is the signature of the noise source at $\mathbf{x}$, $\langle . \rangle$ denotes spatial ensemble average, and $\hat{S}(\omega)$ is the power spectrum of a noise source where it is assumed that $\hat{S}(\omega)$ is the same for all $\mathbf{x}$.

Rewriting equation 1 using uncorrelated noise sources leads to (Wapenaar and Fokkema, 2006)

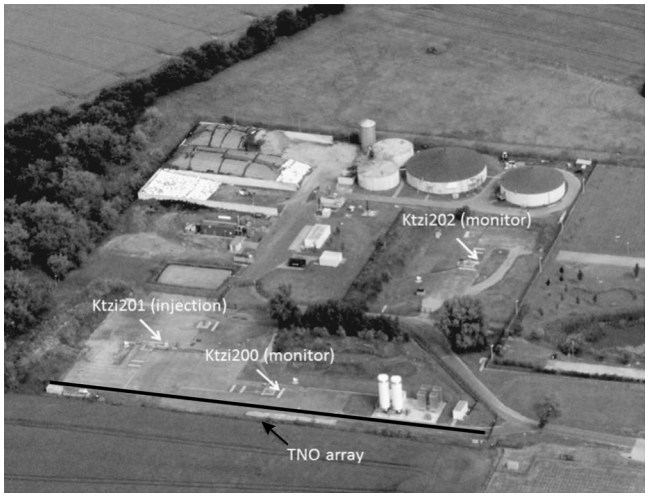

Figure 3. View of the injection site (courtesy of GFZ). The black solid line denotes the approximate 120-m-long east–west-oriented line formed by TNO's surface sensors. The locations of injection well Ktzi201 and the two monitor wells Ktzi200 and Ktzi202 are indicated by the white arrows.

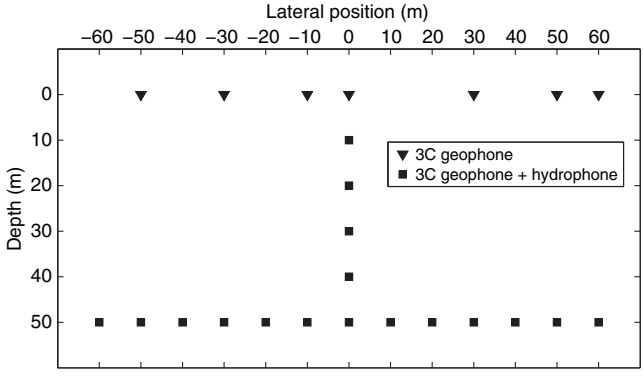

Figure 4. Sketch of the TNO array of permanent seismic sensors installed at the site of Ketzin near the injection well.

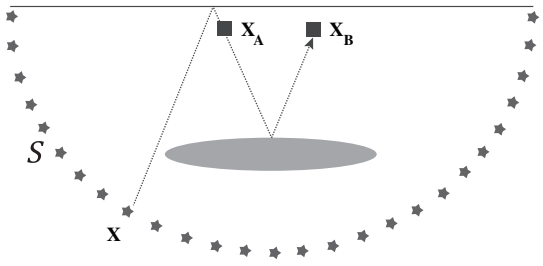

Figure 5. Configuration for ANSI. Passive seismic sources (stars) are regularly distributed along a subsurface boundary S. The virtual seismic response between two buried receivers at positions $\mathbf{x}_A$ and $\mathbf{x}_B$ (boxes) is retrieved by crosscorrelating the individual responses and summing over the source positions x on S. Note that no sources are required at the earth's free surface.

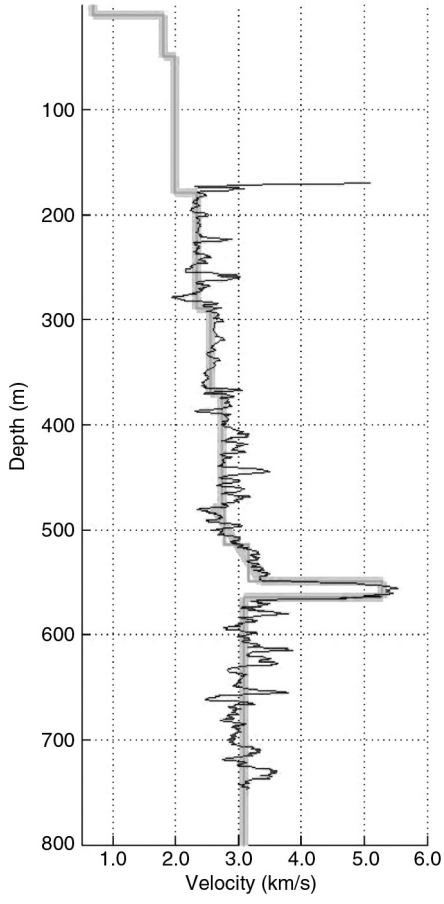

Figure 6. Sonic log (black) and blocked sonic (light gray) of monitor well Ktzi202.

$$\{\hat{G}(\mathbf{x}_B, \mathbf{x}_A, \omega) + \hat{G}^*(\mathbf{x}_B, \mathbf{x}_A, \omega)\}\hat{S}(\omega) \approx \langle \hat{v}^{obs*}(\mathbf{x}_B, \omega)\hat{v}^{obs}(\mathbf{x}_A, \omega)\rangle, \quad (3)$$

where

$$\hat{v}^{obs}(\mathbf{x}_{A,B}, \omega) = \oint_S \hat{G}(\mathbf{x}_{A,B}, \mathbf{x}, \omega)\hat{N}(\mathbf{x}, \omega)d^2\mathbf{x}. \quad (4)$$

Equation 3 relates the seismic response between $\mathbf{x}_A$ and $\mathbf{x}_B$ to the crosscorrelations of long passive wavefields $\hat{v}^{obs}(\mathbf{x}_{A,B}, \omega)$ recorded at $\mathbf{x}_A$ and $\mathbf{x}_B$. Due to the fact that the noise sources are assumed to be mutually uncorrelated, prior separation of the responses is not required before crosscorrelation. This is advantageous if responses from several passive sources are simultaneously recorded at the array, which might effectively occur in the field. Note, however, that it is unlikely that the noise sources would be perfectly mutually uncorrelated. Nevertheless, equation 3 is considered acceptable for ANSI because, often, the noise sources may present a significant lack of correlation or their global transmission responses do not overlap in the passive recordings. In the time domain, the ANSI relation becomes

$$\{\hat{G}(\mathbf{x}_B, \mathbf{x}_A, t) + \hat{G}(\mathbf{x}_B, \mathbf{x}_A, -t)\} \otimes S(t) \approx \langle \hat{v}^{obs}(\mathbf{x}_B, -t) \otimes \hat{v}^{obs}(\mathbf{x}_A, t)\rangle, \quad (5)$$

where $\otimes$ denotes convolution and $S(t)$ is the autocorrelation of the source time functions (signatures) of the noise sources. Note that the right side represents crosscorrelation as time-advanced and time-retarded fields are convolved. The numerical results that we discuss below are based on this relation.

MODELING OF LONG-DURATION PASSIVE MEASUREMENTS

Subsurface model

Various geophysical measurements have been carried out at the CO_2 storage site at Ketzin before and during the injection. Several active seismic surveys were performed on the site to obtain structural and impedance subsurface information. Juhlin et al. (2006, 2007) show the results of a 3D baseline seismic survey acquired in 2005 before the start of the CO_2 injection. As a result, their final migrated image exhibits nearly flat reflectors in the subsurface. Using the permanent array of sensors described in Figure 4, Arts et al. (2011) acquire an active survey and obtain a stacked section that matches the baseline image from Juhlin et al. (2007).

As can be seen from the 3D time-migrated reflection stacks in Figure 2, the Ketzin subsurface underneath the demonstration site is in the first approximation plane, horizontally layered along the east–west direction: The injection site falls approximately on crossline 1100 and inline 1175; the TNO array is oriented approximately east–west. The P-wave velocity model used for the base (0% CO_2) scenario is derived by blocking (a special kind of averaging) of the sonic log readings of well Ktzi202 (Figure 6). The blocked sonic

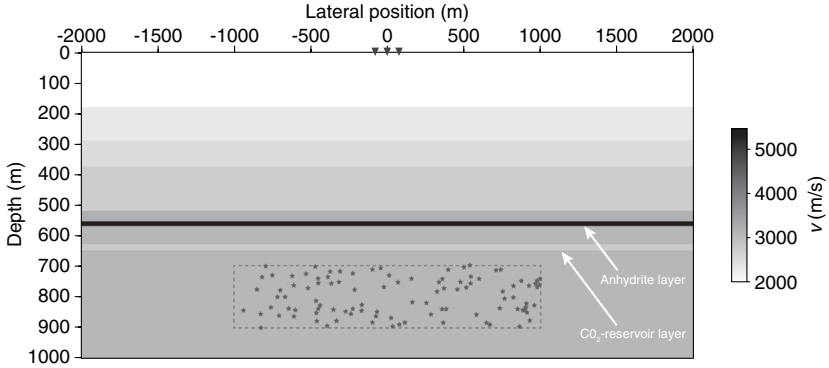

Figure 7. Acoustic velocity model: v denotes P-wave velocity. The triangles on top denote the approximate positions of the leftmost, central, and rightmost surface stations of the array presented in Figure 4. The P-wave velocity in the anhydrite layer is $v = 5300$ m/s. The CO_2 reservoir is modeled as a 20-m-thick layer with an initial P-wave velocity of 2765 m/s (i.e., before the start of injection). The stars mark the positions of 100 noise sources randomly distributed within the region delimited by the dashed lines ($x = [-1000, 1000]$ m and $z = [700, 900]$ m).

Table 1. Base and repeat scenarios of the reservoir velocity v_{res} inside the CO_2 reservoir.

Scenarios	P-wave velocity (m/s)	Decline
Base	$v_{res} = 2765$	0%
Repeat	$v_{res} = 2212$	20%

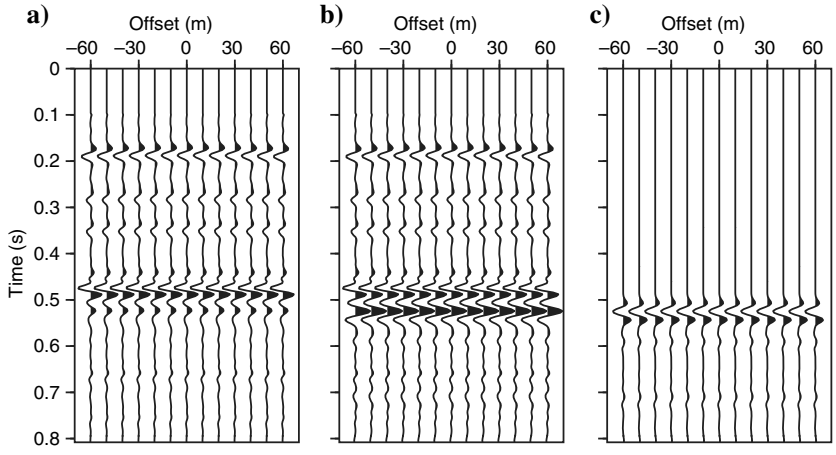

Figure 8. Modeled (a) base and (b) repeat responses from an active source at $(x, z) = (0, 0)$ m and geophones at the surface from −60 to 60 m with 10-m spacing. The modeled responses correspond to the vertical component of the particle velocity. The source signature is the time derivative of a Ricker wavelet with a peak frequency of 20 Hz. (c) The time-lapse difference signal obtained by subtracting (b) from (a).

model exhibits a high-impedance layer (i.e., the anhydrite layer) that produces the strong composite reflection and is mapped as the K2 reflector in the migrated stacks at the injection location (Figure 2). We can observe that the contrasts in the blocked sonic model correspond reasonably well with reflectors in the migrated stacks at the injection location (Figures 2 and 6). Notice that the uppermost 200 m concerns an educated guess of the velocity function because we have no sonic data in this interval. The repeat (CO_2 saturated) scenario is created by applying Gassmann's fluid substitution equation for the reservoir layer.

Based on these observations, we consider that a horizontally layered acoustic earth model is a reasonable representation of the subsurface at the injection site for the geometry of the TNO array. By modeling the wavefield propagation acoustically, we generate passive data free from surface waves because it is desired to retrieve reflections. In practice, surface waves can be eliminated by selection and/or filtering methods prior to crosscorrelation, for example, as proposed by Almagro Vidal et al. (2014).

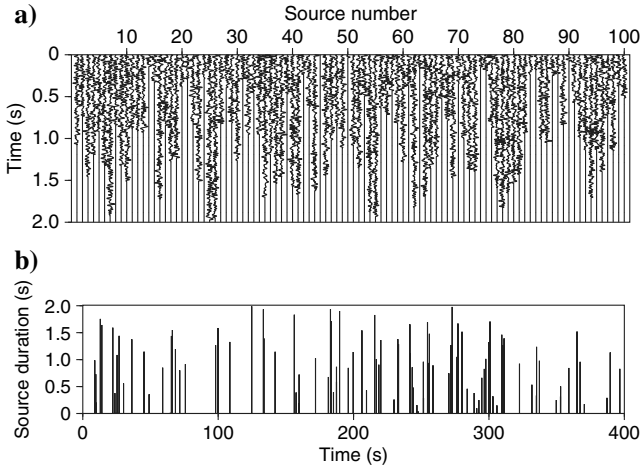

Figure 9. Modeling of the passive noise sources. In this example, 100 sources are triggered during a total modeling time of 400 s. (a) The signatures of 100 noise sources. The duration of the source signals follows a uniform distribution between 0 and 2 s, and their maximum frequency is 50 Hz. (b) The total time window with occurrence times and durations of the source signals.

The P-wave velocities of our model (Figure 7) increase gradually from 1800 to 3000 m/s, until the very high impedance layer at around 550-m depth is reached. This geologic layer corresponds to the impermeable anhydrite formation (Förster et al., 2006) and produces the very strong reflection, K2, in the active data as mentioned above. Because CO_2 is injected at around 80 m below this formation, we model the CO_2 reservoir as a 20-m-thick layer at a 650-m depth with an initial P-wave velocity of 2765 m/s.

During the CO_2 injection, the medium properties are expected to change inside the reservoir. In an acoustic environment, increasing the saturation of CO_2 in the reservoir causes a decrease of its effective P-wave velocity. Arts et al. (2004) observe such velocity changes in time-lapse seismic data acquired during CO_2 storage in a saline aquifer at Sleipner. For our feasibility study of time-lapse ANSI, we consider a repeat scenario that corresponds to a decrease in the P-wave velocity by 20% inside the reservoir layer (see Table 1).

The corresponding base and repeat seismic responses for an active source at $(x, z) = (0, 0)$ m and for receivers at the surface from −60 to 60 m with 10-m spacing are shown in Figure 8a and 8b, respectively. Note, in particular, the strong composite response from the high-impedance layer at around 0.48 s, which does not vary in Figure 8a and 8b. The seismic response matches quite well with the migrated stacks at the injection location, considering the same frequency band and for coincidental surface source and receiver locations (compare with Figure 2). Reflections from the reservoir layer appear just a bit later than the strong-impedance reflection, with higher amplitudes in the repeat case than in the base case. The time-lapse difference signal is shown in Figure 8c and obtained by subtracting the repeat response from the base response. In the difference signal, a clear change can be seen at around 0.52 s that corresponds unambiguously to the impedance decrease of the reservoir. We use this result as a reference to which we compare our ANSI results retrieved from the modeled body-wave noise. This is a reference result because it is obtained from a perfect repetition of an active source at the surface between base and repeat surveys.

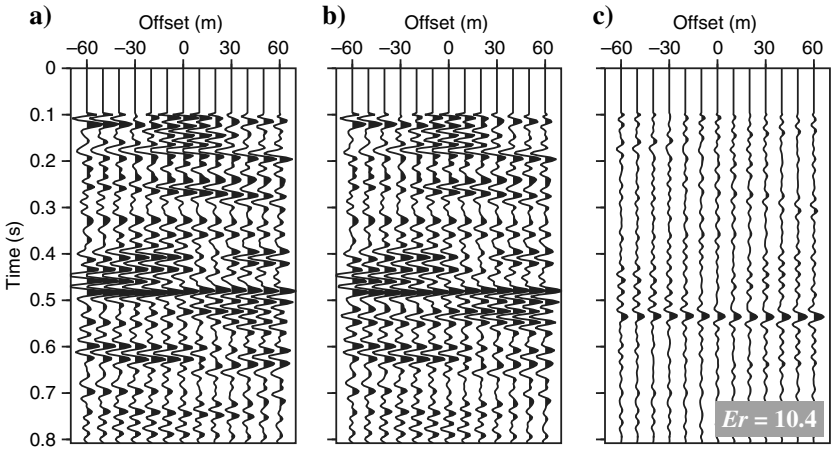

Figure 10. Time-lapse ANSI results using exactly the same distribution of 100 sources for the base and repeat passive surveys. (a) The base VCS gather. (b) The repeat VCS gather. (c) The retrieved time-lapse signal obtained by subtracting (b) from (a).

Modeling of passive data

The simulation of passive seismic measurements is performed using a 2D finite-difference acoustic modeling scheme. We use the program introduced by Thorbecke and Draganov (2011), which enables one to simulate long-duration seismic measurements from band-limited noise sources. The noise sources are modeled via a pseudorandom sequence. In the modeling experiments, the spatial distribution of the noise sources is random within a given source region (Figure 7), whereas the temporal distribution is random within the total modeling time (Figure 9b). The signatures of the noise sources, all with constant maximum amplitude, are randomly generated with, as constraints, a maximum allowed duration and a high-frequency limit (Figure 9a). Consequently, the noise sources do not have identical power spectra (or, equivalently, autocorrelation functions) and are not perfectly

mutually uncorrelated. These two characteristics violate equation 2 and would add crosstalk in the Green's function retrieval. Nevertheless, this crosstalk would have little effect on the retrieved results because the pseudorandom property of the source signatures tends to minimize their mutual correlation. In addition, we expect it to be a more realistic representation of body-wave noise.

In our modeling experiments, ambient-noise measurements are simulated by recording continuously the global transmission responses due to the noise sources. By doing so, we emulate passive field measurements of body-wave noise that may take several months. In the following, *base passive surveys* and *repeat passive surveys* refer to the modeled passive seismic measurements for the base and repeat velocity scenarios, respectively.

RETRIEVED BASE AND REPEAT VIRTUAL SHOT GATHERS

To retrieve a reflection response between receivers at $\mathbf{x}_A$ and $\mathbf{x}_B$, the passive records at these two receivers are crosscorrelated. According to equation 5, this operation results in both the Green's function from $\mathbf{x}_A$ to $\mathbf{x}_B$ (at positive lags) and its time-reverse version (at negative lags), convolved with the autocorrelation of the noise-source signatures. We get the desired retrieved shot response by always taking the causal part of the correlation result (this fixes the sign definition of direct-wave propagation direction). To retrieve a virtual shot gather, we apply these operations to all available $\mathbf{x}_B$ positions while keeping $\mathbf{x}_A$ constant; $\mathbf{x}_A$ is the virtual-source position. In our modeling experiments, we used the position $\mathbf{x}_A = (0, 0)$ m as the virtual-source position. The corresponding record at this receiver (or master trace) is therefore correlated with all 13 traces (from $\mathbf{x}_B = (-60, 0)$ m to $\mathbf{x}_B = (60, 0)$ m with 10-m spacing). We refer to the virtual shot gathers retrieved by ANSI applied to the modeled base and repeat passive surveys as the base and repeat virtual common-shot (VCS) gathers, respectively.

Random distribution of noise sources

We consider an ambient-noise scenario with 100 noise sources randomly active during a time window of 400 s. As shown in Figure 9, the duration of the source signals follows a uniform distribution between 0 and 2 s. The chosen duration is supported by observations from Santonico et al. (2012) and Paap et al. (2013). We choose, for the sake of illustration, to have the source hypocenters randomly distributed in a 2-km-wide region below the reservoir level, as shown in Figure 7 ($x = [-1000, 1000]$ m and $z = [700, 900]$ m). This configuration refers partly to the ideal contour of sources as in Figure 5. Note that because the source region lies vertically below the recording stations, it has the advantage to cover, at least parts of, the stationary-phase regions that will contribute to retrieve the short-offset reflections. For random distributions, the accuracy of the retrieved reflection responses will depend on the source density in the stationary-phase regions (Fan and Snieder, 2009). Inversely, sources on the sides of the model would less likely contribute to the retrieval of reflections because they would illuminate the array with incident angles that are too high.

First, we consider the case in which exactly the same distribution and sequence of noise sources occurs during the base and the repeat passive surveys. The retrieved base and repeat VCS gathers are shown in Figure 10a and 10b. Because the main energy is retrieved at zero time lag and because we are interested in deeper reflections, the first 0.1 s of each panel is muted. The energy at and around zero time-lag represents the temporally and spatially band-limited virtual-source function. Comparison with the base and repeat gathers in Figure 8 shows that the two VCS gathers in Figure 10 contain the strong reflections from the K2 reflector at around 0.48 s. The weaker reflections are also retrieved, but they are overlain by correlation artifacts. These artifacts, though, are retrieved identically in the base and repeat gathers due to the utilization of the same sequence of noise sources. Because of that they cancel almost perfectly in the difference panel (Figure 10c) leaving the clear time-lapse response at the reservoir level. Although the retrieved results

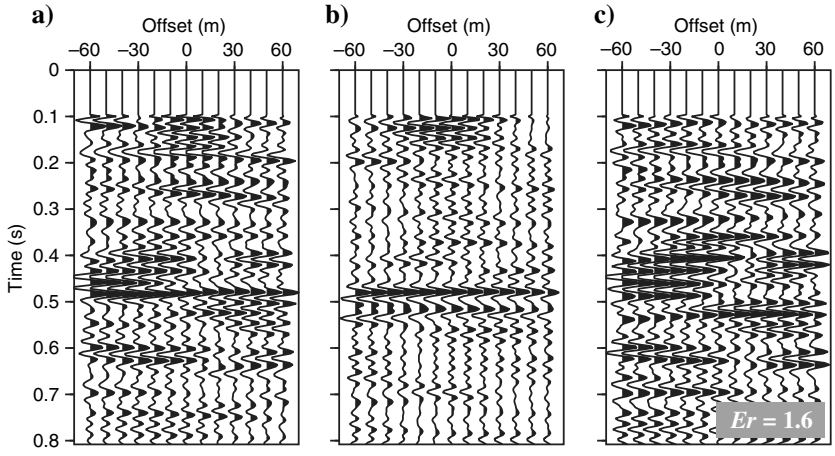

Figure 11. As in Figure 10, but the 100 noise sources have different distributions in the base and the repeat surveys. (a) The base VCS gather. (b) The repeat VCS gather. (c) The retrieved time-lapse signal obtained by subtracting (b) from (a).

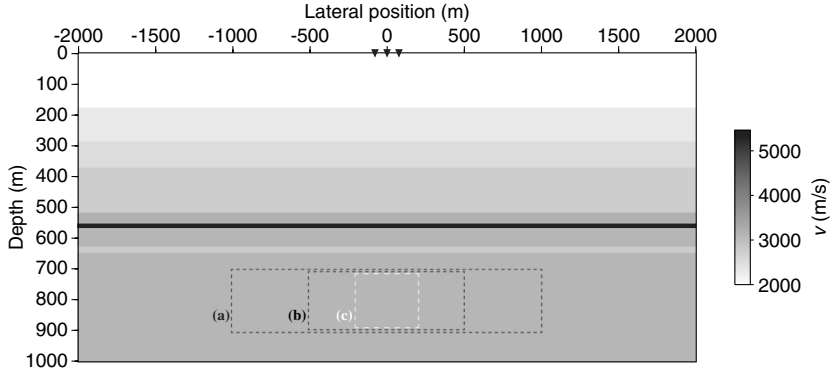

Figure 12. Source regions considered for the modeling experiments: (a) $x = [-1000, 1000]$ m and $z = [700, 900]$ m; (b) $x = [-500, 500]$ m and $z = [700, 900]$ m; and (c) $x = [-200, 200]$ m and $z = [700, 900]$ m.

contain a slightly different wavelet than in the active reference, the time-lapse difference due to the impedance change in the reservoir is clearly obtained by the ANSI.

We quantify the correlation artifacts retrieved together with the expected time-lapse signal by defining the energy ratio:

$$Er = \frac{\frac{1}{Ns}\sum_{i=1}^{Ns} As[i]^2}{\frac{1}{Nb}\sum_{j=1}^{Nb} Ab[j]^2}, \quad (6)$$

where Ns is the number of time samples in the part of the panel in which the time-lapse signal is expected and Nb is the number of time samples in the background part of the panel. Amplitudes $As[i]$ and $Ab[j]$ are the ith time sample in the signal part and the jth time sample in the background part, respectively. The energy ration Er is indicated in the respective figures.

Taking a more realistic case, during the modeling of the repeat passive survey, we now use a different distribution of the noise sources. The number of sources, the source strength, and the source region are kept the same. In this case, the locations of the sources and their excitation times and durations vary between base and repeat surveys. This may lead to some variations in the illumination of the array and in the total recorded energy, the latter being solved with normalization of the crosscorrelated traces. The resulting base and repeat VCS gathers are shown in Figure 11a and 11b, respectively. The repeat VCS gather now contains artifacts that are different from the retrieved artifacts in the base response. This is due to the fact that the respective illuminations of the array do not sufficiently match during the base and the repeat surveys. Significant time-lapse variations of the illumination would occur whenever the spatial density of the noise sources is too low in the considered source region. In this case or when the seismically active region shifts, the retrieved time-lapse difference signal would be polluted with possibly strong time-lapse artifacts, as is the case in Figure 11c. Hence, interpreting the time-lapse response induced by the reservoir becomes impossible. Fan and Snieder (2009) show that, for random distributions, the source density governs the accuracy of the Green's function reconstruction. Based on their conclusions, we foresee that a solution to magnify the time-lapse signal is to have higher spatial density of sources in the considered source region. This can be achieved by considering a smaller source region and/or by capturing the global transmission responses from more noise sources.

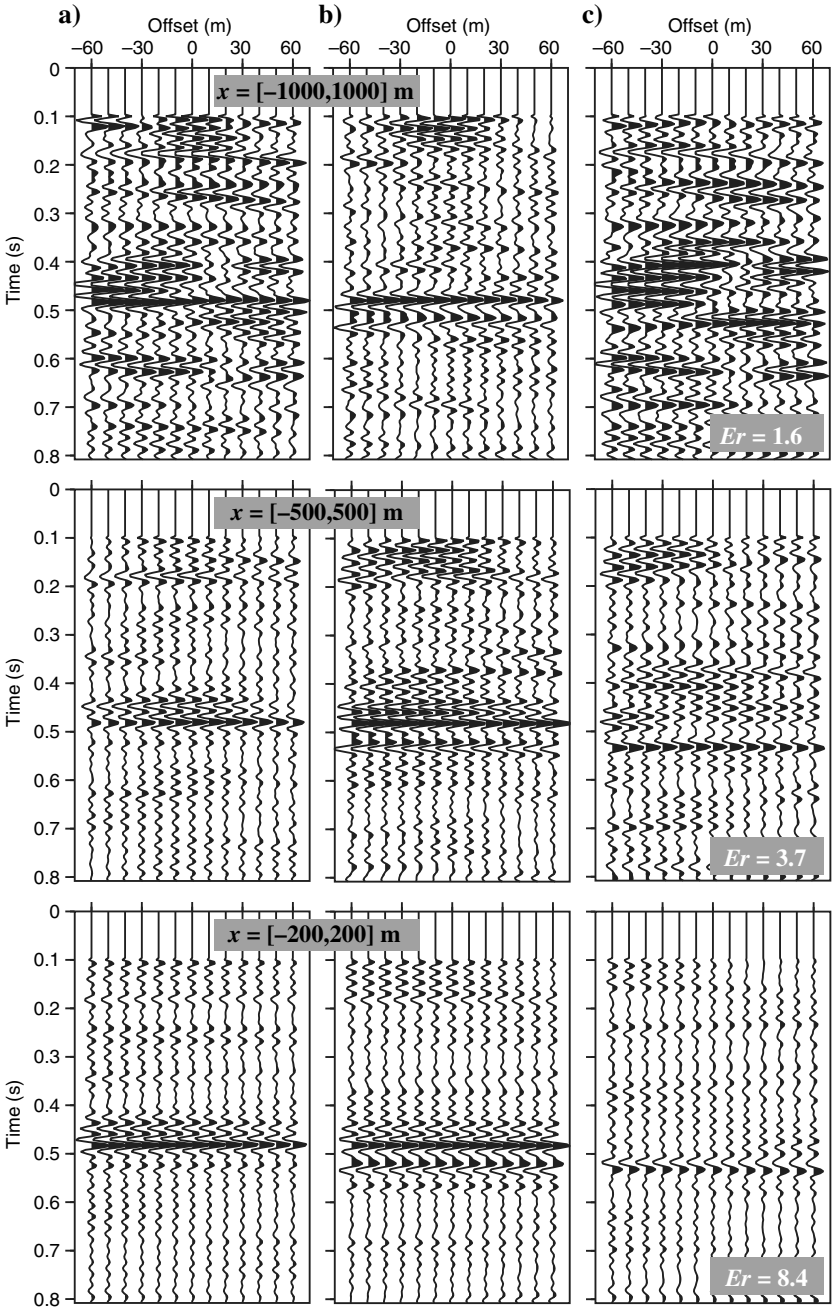

Figure 13. ANSI results for the three different source regions as defined in Figure 12: (a) base and (b) repeat VCS gather and (c) time-lapse difference obtained by subtracting (b) from (a). The number of sources is always 100 for the base as well as for the repeat passive survey. The source-region extent is specified in the upper sections of the base-survey and repeat-survey results.

Spatial extent of the source region

Let us examine the influence of the spatial extent of the source region for a few noise sources that we keep fixed to 100. In practice, this would mean that the recording time is long enough for the base and repeat surveys to capture the response from 100 noise sources. The other source-related parameters are as in Figure 9, but use different realizations for the base and the repeat surveys. We consider three source regions that differ in their spatial extent in the horizontal direction (see Figure 12).

For each of the three regions, we model a base and a repeat passive survey with randomly distributed noise sources. The base and repeat VCS gathers and the corresponding time-lapse

differences are shown in Figure 13. For the case when the source region is 2-km wide (repeated from Figure 11 for comparison convenience), the retrieved reflection response is strongly contaminated with correlation artifacts. Moreover, there are significant variations for these artifacts in the base and repeat retrieved responses, which results in a totally uninterpretable reservoir-related time-lapse signal. For the source region with $x = [-500, 500]$ m, the retrieved VCS gathers exhibit better estimates of the reflection response. In addition, due to the increase of the source density, a better match of the artifacts in the base and repeat gathers is achieved. This leads to an interpretable time-lapse signal from the reservoir. Note, however, that artifacts are still present, and they may be as strong as the target reflections. For the case of a source region with $x = [-200, 200]$ m, the artifacts in the difference panel are further suppressed as a result of increased repeatability of the passive survey.

The results of Figure 13 show the importance of having sufficiently well-repeated illumination during the passive surveys to retrieve a consistent time-lapse signal with ANSI. In practical applications, such repeatable illumination could be achieved by using only parts of the ambient noise that originate from a certain region. Such regions could be chosen using, for example, the illumination-diagnosis procedure that Almagro Vidal et al. (2014) propose for suppression of surface-wave retrieval and better retrieval of reflections.

Number of sources

Let us now examine the influence of the number of noise sources on the retrieved time-lapse difference for a fixed source region. In the field, the number of recorded noise sources during the passive measurements will depend on the intensity of the natural and induced seismic activity. If the occurrence of seismic events is low, a longer listening time would be required to capture more body-wave noise arrivals. Previous work by Xu et al. (2012) suggests that one day of recording may already be sufficient to retrieve reflections at Ketzin. Because we are interested only in time-lapse differences, the required listening time for capturing the needed number of sources may be shorter.

In the bottom ANSI results in Figure 13, the source region is characterized by $x = [-200; 200]$ m, and the number of noise sources is 100 for the base and repeat passive surveys. In the following, we keep the same source region ($x = [-200; 200]$ m), but the number of contributing sources is successively increased to 200 and 500. The new VCS gathers and time-lapse differences are shown in Figure 14. The case shown in the top panels of Figure 14, for which 100 sources are used, is a repetition of the results shown in Figure 13. The time-lapse signal is already coherent at the reservoir level, but surrounding time-lapse artifacts introduce ambiguity as to whether changes have occurred also at other layers. When the number of sources is increased to 200 (see the middle row in Figure 14), some artifacts present in the results for 100 sources are now suppressed. This is due to the fact that the source region is now better sampled by sources in both surveys. Therefore, the total illuminations of the array match better for the base and repeat passive surveys. When the number of sources is increased to 500 (see the bottom row in Figure 14), the time-lapse difference is further improved because the residual artifacts are further suppressed. The obtained time-lapse

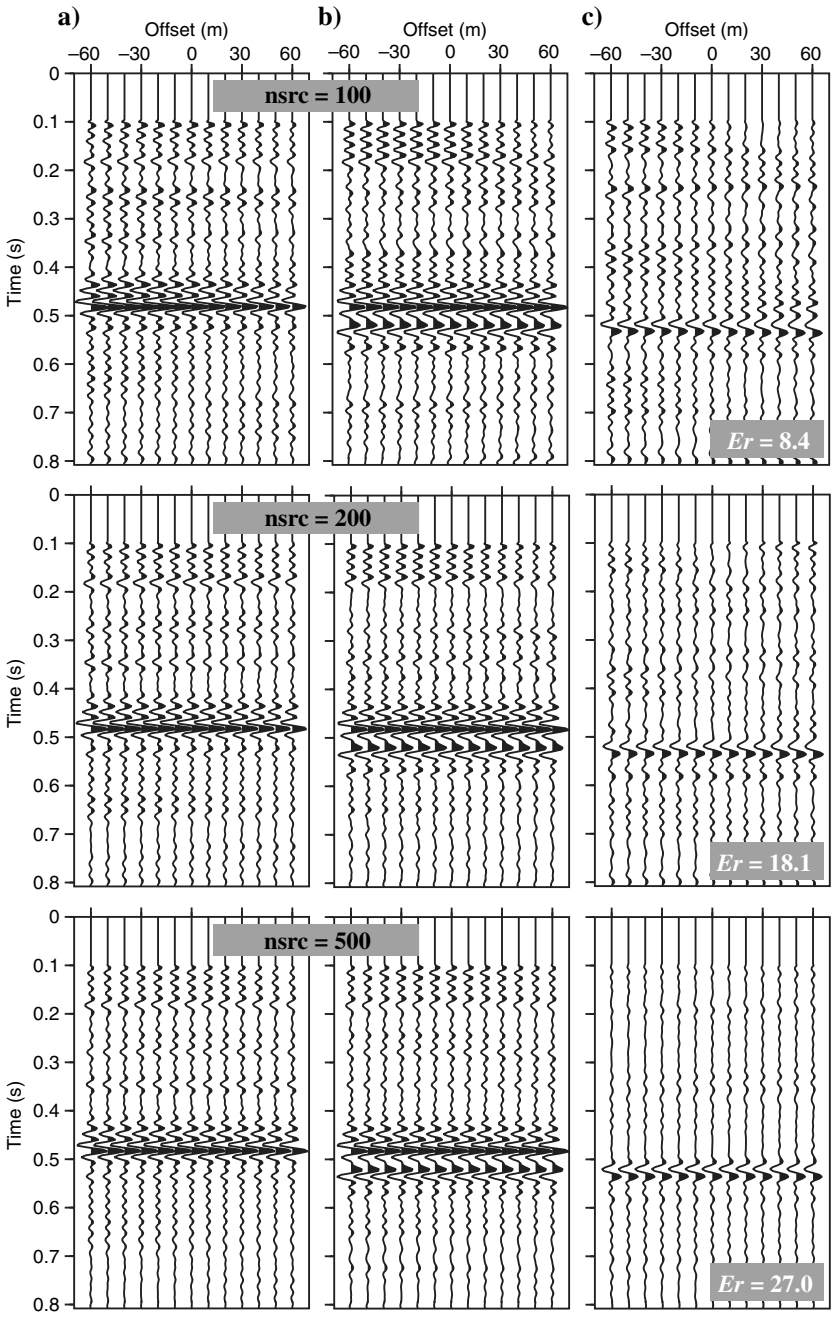

Figure 14. As in Figure 13, except for the changing number of sources, as indicated in the upper sections of the base-survey and repeat-survey results. The source region is kept fixed ($x = [-200; 200]$ m).

difference result compares well with the one obtained from the active source in Figure 8.

Note that even though the number of recorded body-wave noise sources might be the same during the base and repeat passive surveys, the total body-wave energy can vary because two different random sequences of sources would not provide the exact same average durations and spectra. This would result in retrieved VCS gathers for the base and repeat cases whose amplitudes also differ, and thus their difference would be erroneous. A way to solve this problem is to normalize the retrieved gathers before taking their difference with the amplitude of the retrieved reflection from the K2 (strongest reflector) because its properties are not expected to change during storage.

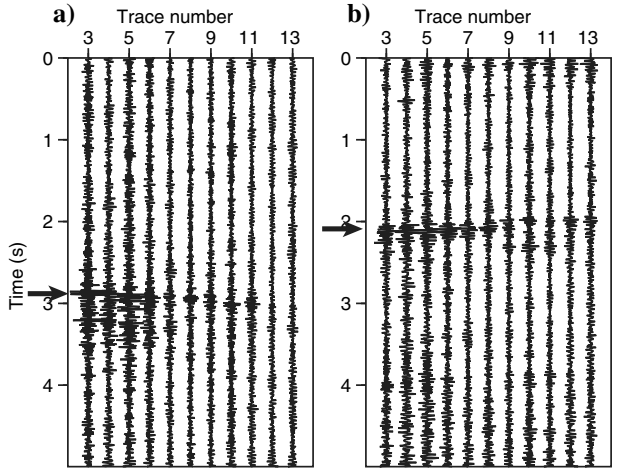

Figure 15. Two panels of 5 s of raw data recorded on 30 January 2012 showing seismic events. The events (indicated by horizontal arrows) were recorded on the vertical component of the geophones buried at 50-m depth and occurred at (a) 3:33 a.m. and (b) 9:49 a.m. The signal was passed between 20–130 Hz, and spiky notch frequencies were suppressed. Notice that the near-horizontal alignment of the dominant events implies near-vertical incidence of the body waves.

COMPARISON WITH FIELD DATA

The numerical tests described in the foregoing section demonstrate that, in the case of the Ketzin subsurface, dominant time-lapse difference information can be obtained from modeled continuous ambient noise (a result that could be expected from noise interferometry theory). This result suggests that ANSI applied on ambient-noise recordings at Ketzin may have potential as a CO_2 monitoring tool as long as seismic reflection events are relevant to the analysis.

Inspired by the encouraging results that Xu et al. (2012) present for 25 h of surface-recorded ambient noise, we set the objective to process, for reflection retrieval with ANSI, large parts of the multi-year TNO data set. From lengthy data-quality assessment sessions, it appeared that it would be most effective to start with the detailed analysis of only a relatively small, but representative, subvolume selection from the total data volume. We therefore use a limited time period: the first three months of 2012. From these data, we use the ambient noise recorded on the vertical component of the geophones and on the hydrophones of the buried horizontal array. In this paper, we will discuss results of an even smaller subset of the data: Only results from a three-day-long period in January 2012 are shown. This is done because the quality of these data is superior to the average data quality in this three-month period, which would mean that stacking results over longer periods would rather deteriorate the quality of the retrieved results than increase it. Figure 15 serves to illustrate this and shows two panels of 5 s of raw data recorded in this three-day period (on 30 January 2012). Nearly vertically incident waves can be identified as isolated near-horizontal events.

The actual field-data recording started, very unfortunately (but for good operational reasons), only after passage of the CO_2 in the reservoir section directly underneath the TNO array. Therefore, a comparison between a base case (i.e., the situation before injection) and a repeat case passive survey cannot be produced. For this reason, the determination from time-lapse difference panels of impedance contrast changes due to increasing CO_2 saturation cannot be carried out. The objective of the field-data study, with the help of numerical simulations, is therefore set to demonstrate that ANSI applied to the Ketzin ambient noise would provide useful body-wave reflection information.

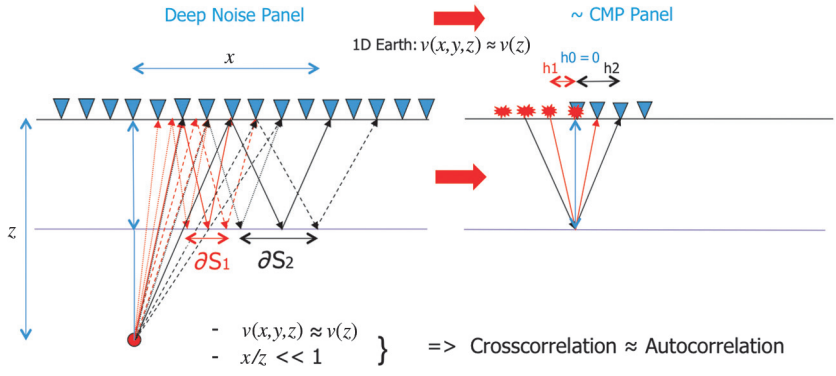

Figure 16. ANSI with noise from relatively deep sources. Assumptions of short offset and a vertically 1D velocity model plus application of the stationary-phase principle provide the opportunity to approximate the virtual common midpoint panel produced with crosscorrelation by the simple straightforward autocorrelation trace at the virtual-source position. On the left only a small subset of contributing raypaths is shown for convenience.

Data processing assumptions and results

Important assumptions underlying the applied field-data processing, briefly described in the following, are that the Ketzin subsurface velocities underneath and in the 3D vicinity of the TNO array vary approximately vertically only (as in Figure 2, bottom) and, in addition, that the virtual-source-to-receiver offsets are much shorter than the reflection-point depths of interest, see Figure 16.

More precisely, the assumption $v(x, y, z) \sim v(z)$ allows us to produce multioffset virtual shot records from common midpoint panels (CMPs) because (1) the CMP concept is valid only for, at most, mild lateral velocity variations and (2) raypaths of reflections in multioffset shot records can be seen as identical, after sorting, to those of

CMPs. Indeed, in laterally homogeneous media, reflection-point information from a multioffset shot gather can be resorted to a CMP. The second mentioned assumption, i.e., the small offset-to-reflection-point-depth ratio condition $x/z \ll 1$, with x virtual source-to-receiver offset and z reflection-point depth, justifies that the multioffset crosscorrelation midpoint gathers (virtual CMPs) can be safely approximated by an autocorrelation of the recording at the virtual-source position chosen at the midpoint (i.e., reflection point) location: offset-dependent amplitude and phase effects are negligible in this case. For the horizontal TNO array, a panel of autocorrelated traces would thus represent a zero-offset reflection section. Note that autocorrelation of passive recordings has been applied before for passive imaging (e.g., Daneshvar et al., 1995).

Prior to data selection, the quality of the continuous field records is inspected, for many different recording time windows, with a TNO-developed diagnostics tool (Zhang et al., 2011). The spectral characteristics of the ambient noise appear to vary largely not only with time but also per recording channel. Based on the findings from the data inspections, we decided to perform the actual processing on selected 24-h records. Autocorrelations are produced for 20-min recordings, a manageable size from a practical point of view, for the vertical-component geophone and hydrophone channels of the array buried at 50-m depth. A running stack is then applied to those 20-min results until 24 h of data are autocorrelated and stacked. The results we show here are produced by applying a 6–10–26–34 Hz Ormsby minimum-phase band-pass filter after correlation. We also apply true-amplitude scaling to correct for spherical divergence, while taking the blocked 1D subsurface velocity model of Figure 6 into account. A few examples of stacked autocorrelation results obtained from the data recorded by the vertical component of the geophones and by the hydrophones are displayed in Figures 17–19.

Figures 17 and 18 show autocorrelation results from the geophones' vertical component and from the hydrophones, respectively, for a three-day period: 28–30 January 2012. Figures 17d and 18d exhibit the stack of the three one-day panels. The vertical-component geophone and hydrophone results show, although in a relatively narrow frequency band, a strong reflectivity sequence around 600 ms. These results are in good agreement with the seismic stack profile, obtained using active sources at the surface (Figure 19a; see also Arts et al. [2011] for a few more active-source data examples), but also with the active-source modeled result in Figure 19d. In the panels in Figure 19, the candidate K2 event is indicated by a gray stripe. The occurrence of the strong reflection at around 600 ms, opposed to 500 ms in Figure 2, can be explained by application of a relatively narrowband Ormsby filter as well as the combined effect of interference of surface-related (virtual-) source and receiver ghosts with the primary reflections due to the burial at 50-m depth: Because of the fact that the receivers are buried at a depth of 50 m, the reflected upgoing waves interfere with downgoing waves reflected at the free surface.

In the active configuration (source at the surface), we get only ghosts on the receiver side. In the passive case, we retrieve a virtual source at a depth of 50 m, which means that we can expect a source ghost, receiver ghosts, and also source-receiver ghosts. These ghosts may (partially) interfere destructively with the primary reflection. The here-described phenomenon may also play a role at shallower depths. But the absence of a strong event, which is present in Figure 19a at around 300 ms, in the correlated results (Figure 19b and 19c) can only be explained by a combination of causes, such as the inaccuracy of the shallow velocity information (above 200-m depth) due to the lack of sonic data, the lack of large offset passive data (present in the active data), and finally, the 3D (crossline) contributions in the active data. The active source line is parallel to the TNO receiver line but does not coincide with it, implying that CMPs are not located in the 2D plane we use for passive data analysis.

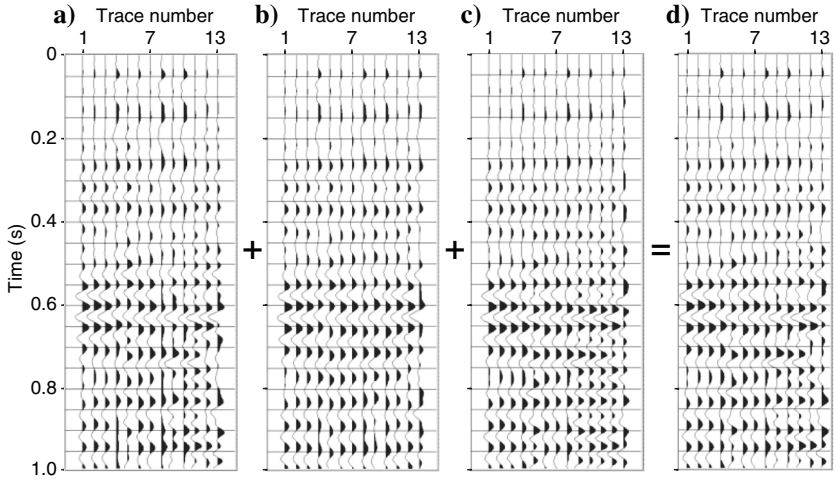

Figure 17. Ketzin field-data autocorrelation panels obtained from 24 h of noise. Results for the vertical component of the geophones using the passive data from (a) 28 January, (b) 29 January, and (c) 30 January (all 2012). Panel (d) is the three-day stack of (a-c).

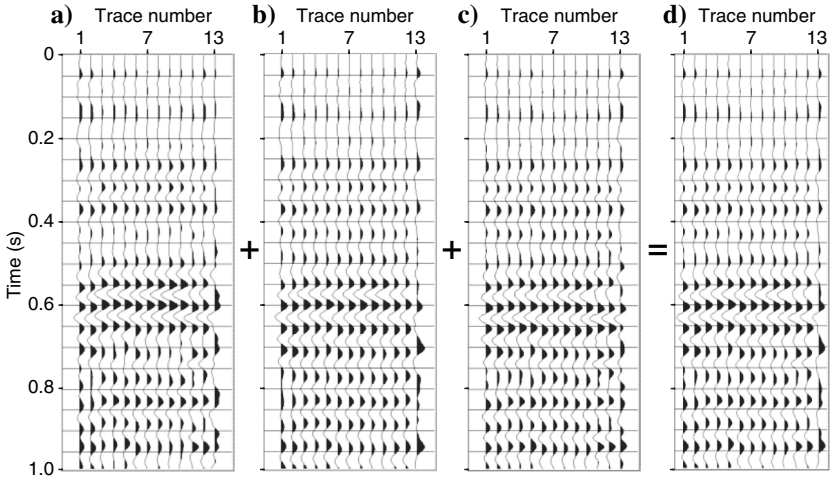

Figure 18. Same as in Figure 17 except for the hydrophones.

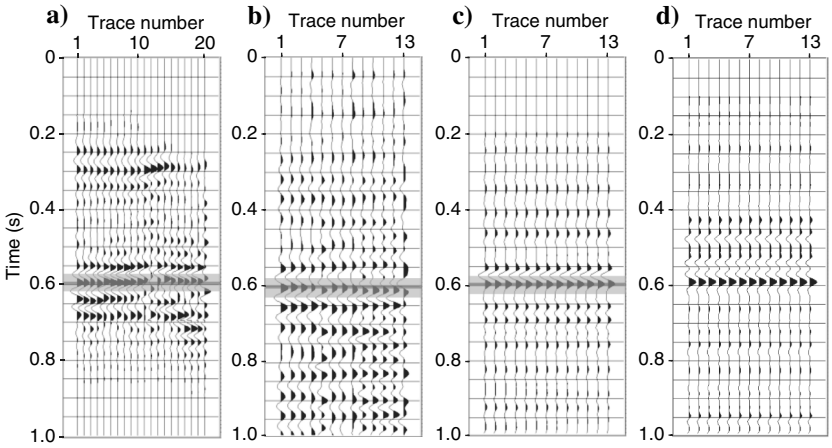

Figure 19. (a) Ketzin field-data stack profile using active sources at the surface and a nearby receiver line parallel to the permanent one of Figure 3. (b) Autocorrelation result using one day of noise recorded on the vertical component of the geophones. (c) Autocorrelation panel obtained from modeled data for the vertical component of the geophones. Panels (a–c) are filtered to the same bandwidth. (d) Active-source modeled response for a source at 50-m depth. The geophones for all cases are at 50-m depth. The candidate location of the K2 event is highlighted with gray stripes.

CONCLUSIONS

We investigated the feasibility of using ANSI for studying impedance changes in a reservoir due to CO_2 storage. We used numerically modeled data and field data from ambient noise recorded by the TNO permanent array at the CO_2 storage site at Ketzin, Germany. For the numerical modeling, we used a horizontally layered subsurface based on a blocked sonic log from Ketzin. To try to detect impedance changes due to CO_2 injection, we modeled a base survey and a repeat survey of ambient noise due to random noise sources in the subsurface. The repeat survey was done after a 20% decline in the velocity at the reservoir. Our numerical results showed that detecting impedance changes on time-lapse difference panels obtained from ANSI by crosscorrelation depends mainly on the repeatability of the illumination of the passive array from the noise sources during the base and repeat surveys. We showed that repeatable illumination for two different realizations of random sources is achieved when the noise-source spatial density for the two surveys is sufficiently high. We achieved this density by limiting the distribution area of the noise sources in the subsurface below the passive array and increasing the number of noise sources. In practice, this would mean applying illumination diagnosis to choose noise from desired directions and recording for a sufficiently long time to ensure a sufficient density of noise sources. We also applied ANSI to three-day-long ambient noise recorded by the TNO field array. Because the recordings started after the CO_2 front had passed the location of the array, time-lapse panels for impedance-change detection could not be obtained. Instead, we applied ANSI to retrieve the reflection response of the subsurface and the CO_2 saturated reservoir. Making use of the relatively short length of the passive array and the lateral homogeneity of the subsurface for this length, we applied ANSI by autocorrelation to retrieve virtual zero-offset traces at all positions of the receivers buried at a 50-m depth. Comparing the obtained results with active-source field and modeled data and with ANSI by autocorrelation results retrieved from the modeled data, we showed a striking correspondence in the retrieved arrival times of the reflections from a large depth interval around the K2 event. We therefore do believe that ANSI provides scope for increased study and application in CO_2 storage projects.

ACKNOWLEDGMENTS

This work is supported by the Division for Earth and Life Sciences (ALW) with financial aid from the Netherlands Organization for Scientific Research (NWO, VIDI grant 864.11.009). The authors would like to thank the colleagues of GFZ Potsdam for their assistance in getting the array installed. Shell, Statoil, RWE, Vattenfall, and E-on are acknowledged for their financial support that made the installation possible. Partners in the European networks CO2GEONET, CGS Europe, and EERA are thanked for their advice and constructive discussions. The Dutch national program CATO-2 is acknowledged for supporting the development of the processing and interpretation workflow for the passive seismic data. Furthermore, we wish to thank (former) TNO colleagues R. Arts (now at GDF Suez), S. Meekes, V. Vandeweijer, and W. Visser for inspiring discussions and useful suggestions. H. Wedemeijer (also of TNO) provided indispensable assistance with field data processing and software development and testing. Finally, the use of the seismic processing package Promax was of great help for the study of the field data.

REFERENCES

Almagro Vidal, C., D. Draganov, J. van der Neut, G. Drijkoningen, and K. Wapenaar, 2014, Retrieval of reflections from ambient noise using illumination diagnosis: Geophysical Journal International, **198**, 1572–1584, doi: 10.1093/gji/ggu164.

Arts, R., O. Eiken, A. Chadwick, P. Zweigel, B. van der Meer, and G. Kirby, 2004, Seismic monitoring at the Sleipner underground CO_2 storage site (North Sea): Geological Society, London Special Publications 233, 181–191, doi: 10.1144/GSL.SP.2004.233.01.12.

Arts, R. J., J. A. C. Meekes, J. H. Brouwer, M. van der Werf, R. P. Noorlandt, B. Paap, W. Visser, V. Vandeweijer, S. Lüth, R. Giese, and J. Maas, 2011, Results of a monitoring pilot with a permanent buried multicomponent seismic array at Ketzin: Energy Procedia, **4**, 3588–3595, doi: 10.1016/j.egypro.2011.02.288.

Bergmann, P., M. Ivandic, B. Norden, C. Rücker, D. Kiessling, S. Lüth, C. Schmidt-Hattenberger, and C. Juhlin, 2014, Combination of seismic reflection and constrained resistivity inversion with an application to 4D imaging of the CO_2 storage site, Ketzin, Germany: Geophysics, **79**, no. 2, B37–B50, doi: 10.1190/geo2013-0131.1.

Claerbout, J. F., 1968, Synthesis of a layered medium from its acoustic transmission response: Geophysics, **33**, 264–269, doi: 10.1190/1.1439927.

Daneshvar, M. R., C. S. Clay, and M. K. Savage, 1995, Passive seismic imaging using microearthquakes: Geophysics, **60**, 1178–1186, doi: 10.1190/1.1443846.

De Ridder, S., and B. Biondi, 2012, Continuous passive seismic monitoring of CCS projects by correlating seismic noise — A feasibility study: 74th Annual International Conference and Exhibition, EAGE, Extended Abstracts, P253.

Draganov, D., X. Campman, J. Thorbecke, A. Verdel, and K. Wapenaar, 2009, Reflection images from ambient seismic noise: Geophysics, **74**, no. 5, A63–A67, doi: 10.1190/1.3193529.

Draganov, D., X. Campman, J. Thorbecke, A. Verdel, and K. Wapenaar, 2013, Seismic exploration-scale velocities and structure from ambient noise (>1 Hz): Journal of Geophysical Research, **118**, 4345–4360, doi: 10.1002/jgrb.50339.

Draganov, D., K. Wapenaar, W. Mulder, J. Singer, and A. Verdel, 2007, Retrieval of reflections from seismic background-noise measurements: Geophysical Research Letters, **34**, L04305, doi: 10.1029/2006GL028735.

Draganov, D., K. Wapenaar, and J. Thorbecke, 2004, Passive seismic imaging in the presence of white noise sources: The Leading Edge, **23**, 889–892, doi: 10.1190/1.1803498.

Fan, Y., and R. Snieder, 2009, Required source distribution for interferometry of waves and diffuse fields: Geophysical Journal International, **179**, 1232–1244, doi: 10.1111/j.1365-246X.2009.04358.x.

Förster, A., R. Giese, C. Juhlin, B. Norden, and N. Springer, CO2SINK Group, 2009, The geology of the CO2SINK site: From regional scale to laboratory scale: Energy Procedia, **1**, 2911–2918, doi: 10.1016/j.egypro.2009.02.066.

Förster, A., B. Norden, K. Zinck-Jørgensen, and P. Frykman, 2006, Baseline characterization of the CO2SINK geological storage site at Ketzin, Germany: Environmental Geosciences, **13**, 145–161, doi: 10.1306/eg.02080605016.

Ivandic, M., C. Juhlin, S. Lüth, P. Bergmann, and A. Kashubin, 2013, Geophysical monitoring of CO_2 at the Ketzin storage site — The results of the second 3D repeat seismic survey: 75th Annual International Conference and Exhibition, EAGE, Extended Abstracts, Th1416.

Juhlin, C., C. Cosma, A. Förster, R. Giese, N. Juhojuntti, H. Kazemeini, B. Norden, and K. Zinck-Jørgensen, 2006, Baseline 3D seismic imaging for the CO2SINK project in the Ketzin area, Germany: Presented at the 8th Greenhouse Gas Technology Conference.

Juhlin, C., R. Giese, K. Zinck-Jørgensen, C. Cosma, H. Kazemeini, N. Juhojuntti, S. Lüth, B. Norden, and A. Förster, 2007, 3D baseline seismics at Ketzin, Germany: The CO2SINK project: Geophysics, **72**, no. 5, B121–B132, doi: 10.1190/1.2754667.

Larose, E., L. Margerin, A. Derode, B. van Tiggelen, M. Campillo, N. Shapiro, A. Paul, L. Stehly, and M. Tanter, 2006, Correlation of random wavefields: An interdisciplinary review: Geophysics, **71**, no. 4, SI11–SI21, doi: 10.1190/1.2213356.

Nakata, N., R. Snieder, T. Tsuji, K. Larner, and T. Matsuoka, 2011, Shear wave imaging from traffic noise using seismic interferometry by cross-coherence: Geophysics, **76**, no. 6, SA97–SA106, doi: 10.1190/geo2010-0188.1.

Paap, B. F., X. Zhang, R. J. Arts, A. R. Verdel, and J. A. C. Meekes, 2013, Continuous passive seismic monitoring of the Ketzin CO_2 injection site, EGU General Assembly: Geophysical Research Abstracts, **15**, 13926.

Ramirez, A. C., and A. B. Weglein, 2009, Green's theorem as a comprehensive framework for data reconstruction, regularization, wavefield separation, seismic interferometry, and wavelet estimation: A tutorial: Geophysics, **74**, no. 6, W35–W62, doi: 10.1190/1.3237118.

Santonico, D., X. Zhang, A. R. Verdel, J. A. C. Meekes, and R. J. Arts, 2012, The first results of continuous passive surface seismic monitoring at the CO_2 injection site of Ketzin: 74th Annual International Conference and Exhibition, EAGE, Extended Abstracts, P017.

Schuster, G. T., 2001, Theory of daylight/interferometric imaging — Tutorial: 63rd Annual International Conference and Exhibition, EAGE, Extended Abstracts, A032.

Schuster, G. T., J. Yu, J. Sheng, and J. Rickett, 2004, Interferometric/daylight seismic imaging: Geophysical Journal International, **157**, 838–852, doi: 10.1111/j.1365-246X.2004.02251.x.

Schuster, G. T., and M. Zhou, 2006, A theoretical overview of model-based and correlation-based redatuming methods: Geophysics, **71**, no. 4, SI103–SI110, doi: 10.1190/1.2208967.

Snieder, R., 2004, Extracting the Green's function from the correlation of coda waves: A derivation based on stationary-phase: Physical Review E, **69**, 046610, doi: 10.1103/PhysRevE.69.046610.

Thorbecke, J. W., and D. Draganov, 2011, Finite-difference modeling experiments for seismic interferometry: Geophysics, **76**, no. 6, H1–H18, doi: 10.1190/geo2010-0039.1.

Ugalde, A., A. Villasenor, B. Gaite, S. Casquero, D. Marti, A. Calahorrano, I. Marzan, R. Corbonell, and A. Perez Estaun, 2013, Passive seismic monitoring of an experimental CO_2 geological storage site in Hontomin (northern Spain): Seismological Research Letters, **84**, 75–84, doi: 10.1785/0220110137.

Wapenaar, K., 2004, Retrieving the elastodynamic Green's function of an arbitrary inhomogeneous medium by cross correlation: Physical Review Letters, **93**, 254301, doi: 10.1103/PhysRevLett.93.254301.

Wapenaar, K., D. Draganov, R. Snieder, X. Campman, and A. Verdel, 2010, Tutorial on seismic interferometry: Part 1 — Basic principles and applications: Geophysics, **75**, no. 5, A195–A209, doi: 10.1190/1.3457445.

Wapenaar, K., and J. Fokkema, 2006, Green's function representations for seismic interferometry: Geophysics, **71**, no. 4, SI33–SI46, doi: 10.1190/1.2213955.

Xu, Z., C. Juhlin, O. Gudmundsson, F. Zhang, C. Yang, A. Kashubin, and S. Lüth, 2012, Reconstruction of subsurface structure from ambient seismic noise: An example from Ketzin, Germany: Geophysical Journal International, **189**, 1085–1102, doi: 10.1111/j.1365-246X.2012.05411.x.

Zhang, X., J. H. Brouwer, J. A. C. Meekes, and R. J. Arts, 2011, Passive seismic monitoring in two carbon sequestration sites, a data driven approach: 73rd Annual International Conference and Exhibition, EAGE, Extended Abstracts, P036.